CORE
Metadata, citation and similar papers at core.ac.uk
Provided by Periodica Polytechnica (Budapest University of Technology and Economics)

168 | https://doi.org/10.3311/PPci.13249
Creative Commons Attribution

Periodica Polytechnica Civil Engineering, 63(1), pp. 168–183, 2019

A micromechanical Sliding-Damage Model Under Dynamic Compressive Loading

Mohammad Hossein Ahmadi[1], Hamed Molladavoodi[1*]

[1] Department of Mining; Rock mechanics
Faculty of Mining and Metallurgical Engineering,
Amirkabir University of Technology
424 Hafez Ave, Tehran, Iran
* Corresponding author, e-mail: davoodi@aut.ac.ir

Received: 03 October 2018, Accepted: 16 November 2018, Published online: 14 January 2019

Abstract

For most rock materials, there exists a strong coupling between plastic flow caused by sliding along micro-crack faces and damage evolution due to nucleation and growth of wing-cracks. The aim of this article is to develop the self-consistent based micromechanical model by taking into account the coupling between frictional sliding and damage process under dynamic compressive loading. The developed model algorithm was programmed in the commercial finite difference software environment for numerical simulation of rock material to investigate the relationship between the mechanical behaviour and microstructure. Eventually while the stress intensity factor at flaw tips exceeds the material fracture toughness, the wing-cracks are sprouted and damage evolution occurs. For frictional closed cracks, an appropriate criterion for the onset of frictional sliding along micro-cracks was proposed in this paper. Also, plastic strain increments were determined by the flow rule, consistency condition and normality rule within the thermodynamic framework. The simulation results demonstrate that the developed micromechanical model can adequately reproduce many features of the rock behaviour such as hardening prior to the peak strength, softening in post-peak region, damage induced by wing-cracks and irreversible deformations caused by frictional sliding along micro-cracks. Furthermore, the softening behaviour of material in post-peak region is affected and the material undergoes higher values of strains and damage up to the residual strength. Therefore, the rock sample simulation with the coupled frictional sliding-damage model could increase plasticity and ductility of the rock in post-peak region because of regarding plastic strains caused by the frictional sliding along micro-cracks.

Keywords

frictional sliding, damage evolution, stress intensity factor, homogenization, self-consistent

1 Introduction

Under compression dominated loading, frictional sliding along closed micro-crack faces and propagation of micro-cracks are commonly considered as main dissipative mechanisms that govern inelastic deformation, damage evolution and progressive failure of cohesive geo-materials [1]. The dominant micro-mechanism that commonly characterizes damage in brittle materials is attributed to the frictional sliding on pre-existing micro-cracks faces and presence of intrinsic flaws such as micro-crack, pores and mismatches in grain boundaries. The frictional sliding and micro-crack growth leading to damage evolution are inherently coupled each other during irreversible processes involving the dissipation of energy and the evolution of microstructure [2, 3]. Due to the preferential direction of the wing-crack nucleation from initial flaw tips, anisotropy and volume dilatancy are induced in damaged material by damage accumulation [4].

Generally, two kinds of damage models are commonly implemented in the literature to describe mechanical deterioration, softening and damage processes. The first type is the phenomenological damage model, and the other consists of models based on the micro-mechanical approaches. In the framework of phenomenological damage models, the material free energy is interpreted as a function of a number of internal variables, such as plastic strain, together with a scalar variable representing isotropic damage, or a second or fourth order tensor representing anisotropic damage. Actual physical mechanisms e.g. unilateral

Cite this article as: Ahmadi, M. H., Molladavoodi, H. "A Micromechanical Sliding-Damage Model Under Dynamic Compressive Loading", Periodica Polytechnica Civil Engineering, 63(1), pp. 168–183, 2019. https://doi.org/10.3311/PPci.13249

effects due to opening and closure of micro-cracks, coupling between friction and damage on the crack faces, as well as interactions between cracks that have fundamental role in overall materials behaviour and damage due to cracks propagation are difficult to take into account in this kind of the model. Furthermore, a large number of input parameters have usually to be determined in phenomenological damage models, and many of them have physically unclear sense. In order to overcome shortcomings of phenomenological damage models, micromechanical damage models have been proposed. In micromechanical damage models, physical mechanisms are scaled from micro-scale to macroscopic behaviour with effective homogenized material properties.

Initial micromechanical damage models are generally limited to dilute distribution of micro-cracks and then are not able to take into account interaction between micro-cracks. Chen et al. (1996) developed a micromechanical damage model under biaxial dynamic compressive loading, without considering the micro-cracks interaction, which randomly distributed sliding micro-cracks activate when the mode-I stress intensity factor reaches its critical value [5, 6]. Horii and Nemat-Nasser (1986) developed a damage model specifically for closed cracks with frictional sliding on the crack interface, which consider the dilute distribution of micro-cracks for materials under dynamic compression loading. The dilute scheme has been used in various works to determine the effective properties of micro-cracked materials, e.g. [7, 8, 9, 10, 11, 12, 13, 14and 15].

In order to overcome the shortcomings of dilute distribution, other Eshelby-based homogenization procedures such as Mori-Tanaka (1973), Ponte-Castaneda and Willis (1995) and self-consistent have been implemented in the literature [15, 16].

Zhu et al. (2008, 2011) used the Ponte-Castaneda and Willis (*PCW*) (1995) and Mori-Tanaka (1973) homogenization schemes to study the materials behaviour with closed frictional micro-cracks under compressive loading [17, 18]. In homogenization with *PCW* and Mori-Tanaka schemes, the materials containing pre-existing micro-cracks are analyzed as the matrix and micro-cracks composition. These researchers proposed a formulation including frictional sliding along micro-cracks associated with damage evolution for rock containing micro-cracks under compressive loading. It is largely admitted that rational determination of damage evolution law is still one of the open issues in this kind of micromechanical damage models. Although damage criteria based on strain energy release rate have been widely adopted as a compromise, the damage resistance function involved therein is still empirical by now [1].

On the other hand, Paliwal and Ramesh (2008) established a micromechanical damage model based on the self-consistent homogenization scheme accounted for two-dimensional slit-like micro-cracks embedded in elliptical inclusion surrounded by homogenized solid matrix. This model is capable of capturing the influence of the statistically pre-existing flaws distribution and the applied strain rate on the rock response [19].

Graham-Brady (2010) developed Paliwal and Ramesh (2008) model and suppose that each element can be treated as a meso-scale continuum with constitutive properties that reflect the characteristics of the underlying microstructure. For this purpose, Graham-Brady (2010) utilized a method that employed probability distributions to these element properties [20]. Katcoff and Graham-Brady (2014) developed the Paliwal and Ramesh (2008) model to study the compressive dynamic failure of brittle materials with circular flaws [21].

In compared with Zhu et al. (2008, 2011) models, the damage evolution law in models based on the work of Paliwal and Ramesh (2008) is also determined rationally based on the dynamic fracture mechanics principle.

However, in compared with Zhu et al. (2008, 2011) and Qi et al. (2016) models based on the *PCW* and Mori-Tanaka homogenization schemes, the coupled micro-crack frictional sliding and damage evolution has not yet implemented in the micromechanical damage models based on the self-consistent homogenization scheme [1]. Although Hu et al. (2015) proposed a plastic-damage model based on the self-consistent homogenization scheme, matrix plastic strain due to dislocation in crystalline network is only considered in this model and material degradation and inelastic deformation are more popularly characterized separately [23].

Nemat-Nasser and Obata (1988) developed a micromechanical damage model for calculation of dilitancy in brittle materials. They were supposed that the total strain consists of an elastic strain due to the elastic deformation of the matrix, plus an inelastic strain due to slip and dilatancy of the preexisting flaws, accompanied by inelastic strain due to micro-cracking. The computed mode-*I* stress intensity factor in theirs works related to a pair of collinear concentrated forces (F) denoted by (K_I) and the mode-*I* stress intensity factor associated with the gaps and in the

presence of applied stresses denoted by (K_I'). In the suggested damage model by Nemat-Nasser and Obata (1988), the total inelastic strain were calculated based on complex physical phenomena in micro-flaw tips e.g. micro-crack surfaces, back slipping and wedge effect. The new researchers used the Nemat-Nasser and Obata (1988) formulation for considerations of inelastic strain and specified the condition for micro-crack surface sliding and coupling between sliding and damage accumulation [40].

Ayyagari et al. (2018) proposed a three-dimensional generalized anisotropic constitutive model for brittle solids contain of the spatial evolution of planar wing-cracks subjected to dynamic compressive loading. They are assumed self-consistent scheme for accounting crack interactions for in the compliance measuring. Also the coupling between the planar flaw and the wing-crack is considered within the definition of second-order damage tensor and was found effective in describing the contribution of damage to compression-induced dilation Ayyagari et.al (2018) is defined a fully three-dimensional anisotropic compliance tensor and evaluated considering the wing-crack mechanism, using a mixed-approach. They were expressed the crack sliding displacement due to micro-cracks surfaces sliding and damage evolution in terms of the wedging force, the principal stress, and the wing-crack and crack sizes [22].

Liu and Graham-Brady (2016), Improved the over previously proposed models suggested by Nemat-Nasser and Obata (1988). They were proposed a physics-based closed-form solution for the instantaneous compliance of a wing-crack damaged material under compressive loading, which has been verified and parameterized through a periodic unit-cell finite element model. In compared to previous work studying the wing-crack model under compressive load, such as Nemat-Nasser and Obata (1988) , the work done by Liu and Graham-Brady (2016), takes the pre-existing flaw into account when defining the wing-crack model, instead of further simplifying it by a straight line crack. The straight line crack model leads to a very limited increment of the compliance along the loading direction, and thus is not an appropriate equivalent model for the wing-crack problem [41].

The aim of this study is to develop the micro-mechanical damage model originally proposed by Paliwal and Ramesh (2008) to take into account coupling between frictional sliding along micro-cracks and damage due to micro-cracking under dynamic compressive loading.

The developed model in this paper incorporates the plastic deformations due to frictional sliding along closed micro-cracks surfaces accompanied by volumetric dilatancy and damage evolution as a result of wing-crack nucleation from flaw tips.

In this way, shear plastic strains due to frictional sliding along micro-crack faces lead to increase the stress intensity factor at flaws tips. When the stress intensity factor in mode-I of loading reaches the critical value (toughness), growth and coalescence of micro-cracks occur via nucleation of wing-cracks from the pre-existing flaw tips.

The proposed coupling between frictional sliding along closed micro-crack faces and damage evolution is formulated in the framework of a micromechanical model based on the self-consistent homogenization scheme which was programmed and implemented into a commercial code. Accordingly, the proposed model was applied to the simulation of brittle rocks behaviour under dynamic loading.

The simulated stress-strain curves based on the original model of Paliwal and Ramesh (2008) and the proposed model in this paper were investigated and compared under applied high strain rate.

2 Description of theoretical framework

2.1 Self-consistent homogenization scheme (SCS)

Brittle materials like rock inherently have distributed flaws that are weaken links and lead to mechanical properties deterioration under applied loading. Fig. 1 demonstrates a representative volume element () of material containing cracks with randomly sizes and orientation, occupying a domain limited by its external boundary surface. is used for communication between macro and micro scales of material behaviours. The homogenization process for brittle rock materials containing distribution of in-homogeneities in solid matrix is illustrated in Fig. 1.

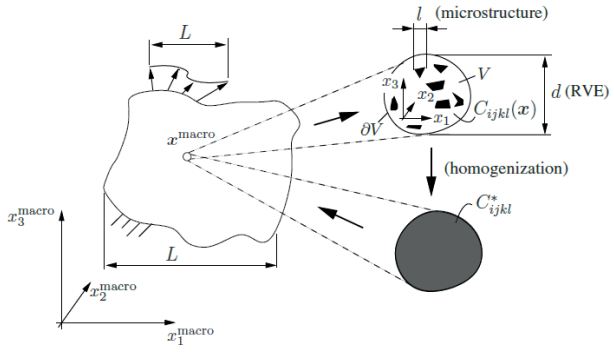

Fig. 1 Homogenization process from micro to macro scale [24]

In a situation that the micro-cracks are close to each other, the self-consistent scheme can be used to determine the effective mechanical properties [25].

According to Fig. 2, in self-consistent scheme it is assumed the presence of an elliptical inclusion surrounding each individual flaw inside of which the material is undamaged. Material outside of the ellipse has the effective homogenized properties accounting for the damage associated with the entire flaw population. The interactions among different flaw families are accounted through the means of crack-matrix-effective-medium approach, which the self-consistent scheme plays a crucial role in determining the local (effective) stress field around the individual flaws. Budiansky and O'Connell (1976) suggested effective Young modules and shear modulus for calculation of damaged matrix [19]:

$$\begin{aligned} &\bar{E} = E \cdot f(v,\Omega), \bar{G} = G \cdot g(v,\Omega), \\ &f(v,\Omega) = \left(1 - \frac{\pi^2}{30}(1+v)(5-4v)\Omega\right), \\ &g(v,\Omega) = \left(1 - \frac{\pi^2}{60}(10-7v)\Omega\right), \end{aligned} \tag{1}$$

here, E and G are the Young's and shear modulus of the pristine material, respectively. Also, v and Ω are the Poisson's ratio and damage parameter, respectively. Meanwhile the effective Poisson's ratio was assumed constant during damage process [19]. Van and Vasharhelyi (2014) calculated deformation modulus of rock mass from the *GSI* value and disturbance factor. In fact, if the deformation modulus of the intact rock (E) is known, the damaged modulus of rock mass ($\bar{E}$) can be determined from disturbance factor that plays the damage parameter roles [42, 44].

2.2 Damage parameter

All of rock materials contain intrinsic flaws that have a different sizes and orientation. According to the weakest link theory under quasi-static loading condition some of the large flaws in the material are activated that affect significantly overall behaviour of material. In other words, small flaws within the material do not activate crack growth, and failure is therefore controlled by large size flaws. In contrast with static loading, under dynamic loading the weakest link theory is not applicable and the whole families of the flaws participate to the mechanical response of brittle solids [26].

The parameter (Ω) is used for assessment of the damage in material under applied loading. The damage parameter in material depends on micro-cracks characteristics such as initial length ($2s$), orientation (φ), areal density (η) and wing-crack length (l). As brittle materials like rock contain distributed micro-cracks with different size and orientation, it could be expressed by statistical functions as follows [19]:

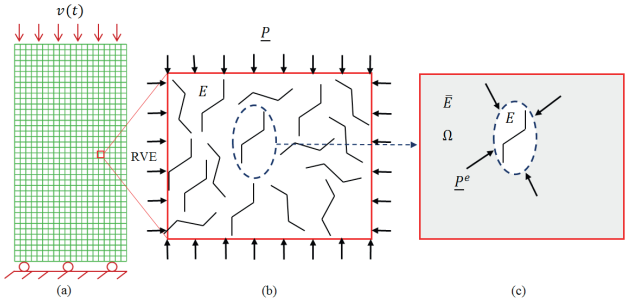

Fig. 2 Self-consistent scheme a) Numerical model, b) RVE, c) Elliptical inclusion surrounding individual flaw

$$\Omega = \int \eta l^2 g(s) f(\varphi)\ dsd\varphi \tag{2}$$

The expresses of $g(s)$ and $f(\varphi)$ are size and orientation statistical distribution functions respectively. For simplicity, the special case of a material whose all flaws have uniform distribution of size and orientation in two-dimensional space is assumed throughout this paper. Therefore, $f(\varphi) = \delta(\varphi - 50.7°)$ is selected for distribution of orientation because it is the most critical orientation under universal compressive loading.

This assumption does not affect the general trends in the proposed model regarding coupling frictional sliding along micro-cracks and damage evolution. In the situation with uniform distribution of size and orientation, the Eq. (2) can be summarized as:

$$\Omega = \eta l^2, \tag{3}$$

Accordingly, the damage parameter evolution can be calculated as following:

$$\dot{\Omega} = 2\eta l \dot{l}, \tag{4}$$

Ghasempour et al. (2017) was considered exponential function for calculation of damage parameter. The damage parameter used in this method begins to increase from yielding (Ω = 0) to failure (Ω = 1). The damaged deformation modulus related to intact deformation modulus as: ($\Omega = 1 - \bar{E}/E$) [43].

2.3 Review of the self-consistent based micromechanical damage model

In this section, the micromechanical damage model formulation based on the self-consistent homogenization scheme is reviewed briefly. The basic idea is that the

individual micro-crack is embedded in an elastic ellipsoidal inclusion surrounded by damaged matrix, and each micro-crack experiences an effective local stress field different from that acts on isolated cracks [19]. Rock material is assumed to be under remote biaxial compressive loading $\underline{P}$ as follows:

$$\underline{P} = [\sigma_{11} \quad \sigma_{22} \quad 0]^T \tag{5}$$

According to Fig. 3, the micro-crack tractions due to remote compressive loading include traction imposed on the initial closed flaw (t_s') and tensile traction applied on wing-cracks (t_w') surfaces [19].

The problem of a micro-crack embedded in elliptical inclusion surrounded by effective homogenized material under compressive loading can be decomposed into two sub-problems according to Fig. 4. In the first sub-problem (Fig. 4(a)), the imaginary micro-crack is inside the elliptical inclusion surrounded by effective homogenized matrix under the same remote biaxial loading as the original problem.

In an undamaged matrix, the local stress imposed on the elliptical inclusion is the same as the remote stress. However, with damaged matrix, the elastic properties of the effective homogenized matrix degrade, causing an elastic properties mismatch at the matrix–ellipsoidal inclusion boundaries. This mismatch leads to a local stress state that differs from the far-field stress state) [27].

In this paper, the methods introduced by Graham-Brady et al. (2015) were implemented to calculate the local stress field ($\underline{P}^e$) imposed on the elliptical inclusion containing an isolated micro-crack as a function of the global principal stress tensor ($\underline{P}$):

$$\underline{P}^e = \underline{\underline{B}} \cdot \underline{P}, \quad \underline{P}^e = \left[\sigma_{11}^e \quad \sigma_{22}^e \quad \sigma_{12}^e\right]^T, \tag{6}$$

The determination of $\underline{\underline{B}}$ is dependent on the undamaged stiffness tensor for the elliptical inclusion (E), stiffness tensor for the damaged matrix material ($\bar{E}$), Eshelby tensor ($\mathbb{S}$) and elliptical inclusion dimensions as described in the Appendix A.

The traction in the first sub-problem ($\underline{t}^r$) shown in Fig. 5 is decomposed into the traction on imaginary micro-crack planes ($\underline{t}_s^r$) and traction on wing-crack surface ($\underline{t}_w^r$), arising from the local stress field ($\underline{P}^e$) acts on the ellipsoidal inclusion boundaries. The traction $\underline{t}^{eff}$ in the second sub-problem shown in Fig. 4(b) causes inelastic deformation and damage evolution. The traction $\underline{t}^{eff}$ must be determined in the manner that satisfies the superposition principle of two sub-problems as follows:

$$\underline{t}' = \underline{t}^r + \underline{t}^{eff}, \tag{7}$$

As illustrated in Fig. 5, both tractions ($\underline{t}_s^r$ and $\underline{t}_w^r$) can be decomposed into the components directed perpendicular and parallel to the surfaces of imaginary micro-cracks, respectively. According to Fig. 5, the components directed perpendicular and parallel to the surface of imaginary micro-cracks in the first sub-problem are calculated through the stress transformation equation as follows:

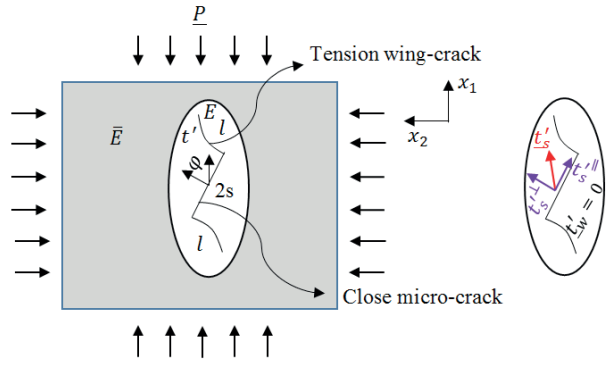

Fig. 3 Schematic illustrations of equivalent medium and tractions acted on initial micro-crack and wing-cracks under remote biaxial loading ($\underline{P}$) [19]

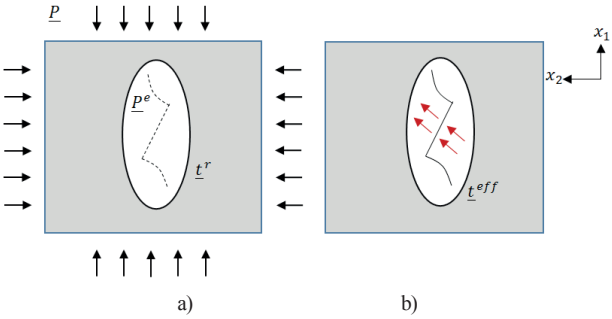

Fig. 4 Decomposition of the original problem shown in Fig. 3, into two sub-problems based on the superposition principle [19]

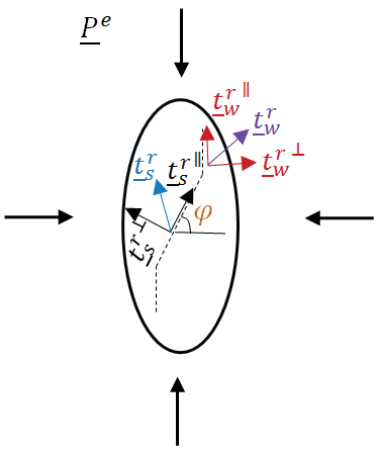

Fig. 5 Decomposition of traction $\underline{t}^r$ applied on the imaginary micro-crack planes in the first sub-problem [19]

$$\underline{t}_s^r \begin{cases} \left(\underline{t}_s^r\right)^{\parallel} = \frac{1}{2}\left(\sigma_{11}^e - \sigma_{22}^e\right)\sin 2\varphi + \sigma_{12}^e \cos 2\varphi \\ \left(\underline{t}_s^r\right)^{\perp} = \sigma_{11}^e \cos^2\varphi + \sigma_{22}^e \sin^2\varphi + \sigma_{12}^e \sin 2\varphi \end{cases} \tag{8}$$

Furthermore, the vertical and parallel components of the traction applied on the wing-crack surface ($\underline{t}_w^r$) can be obtained as follows:

$$\underline{t}_w^r \begin{cases} \left(\underline{t}_w^r\right)^{\parallel} = \sigma_{12}^e \\ \left(\underline{t}_w^r\right)^{\perp} = \sigma_{22}^e \end{cases}, \tag{9}$$

The superscripts "⊥" and "||" indicate the directions perpendicular and parallel to the surfaces, respectively. Since in the second sub-problem the initial micro-crack surface in the normal direction is traction free $\left(\underline{t}_s^{eff}\right)^{\perp} = 0$, the normal component of the resolved traction $(t_s')^{\perp}$ illustrated in Fig. 3 is only due to the first sub-problem and equals the normal component of ($\underline{t}_s^r$). If the Mohr-Coulomb type criterion is applied for frictional sliding along closed micro-cracks, the following expression can be written for the components of traction acting on the sliding micro-crack surfaces:

$$t_s' \begin{cases} \left(t_s'\right)^{\parallel} = \tau c - \mu\left(t_s'\right)^{\perp} = \tau c - \mu\left(\underline{t}_s^r\right)^{\perp} \\ \left(t_s'\right)^{\perp} = \left(\underline{t}_s^r\right)^{\perp} \end{cases}, \tag{10}$$

where μ is the dry friction coefficient for the closed flaws and τ_c is the cohesion. In the second sub-problem illustrated in Fig. 4(b), the effective tractions on flaw surfaces leading to inelastic deformation and damage evolution can be determined based on satisfying the superposition principle of two sub-problems. The effective traction components in the second sub-problem are depicted in Fig. 6. The effective traction $\underline{t}_s^{eff}$ imposed on the initial micro-crack surface causes frictional sliding along micro-cracks. The effective traction $\underline{t}_w^{eff}$ is also applied to the wing-crack surfaces, leading to wing-crack opening and rock damage. The following equation can be written by using the Eqs. (8) to (10):

$$\underline{t}_s^{eff} \begin{cases} \left(\underline{t}_s^{eff}\right)^{\perp} = \left(t_s'\right)^{\perp} - \left(\underline{t}_s^r\right)^{\perp} \\ \left(\underline{t}_s^{eff}\right)^{\parallel} = \left(t_s'\right) - \left(\underline{t}_s^r\right)^{\parallel} = \tau_c - \mu\left(t_s'\right)^{\perp} - \left(\underline{t}_s^r\right)^{\parallel} = \tau^{eff} \end{cases} \tag{11}$$

Because of wing-cracks opening during damage process, it can be assumed that and the effective traction imposed on the wing-crack surfaces can be written as:

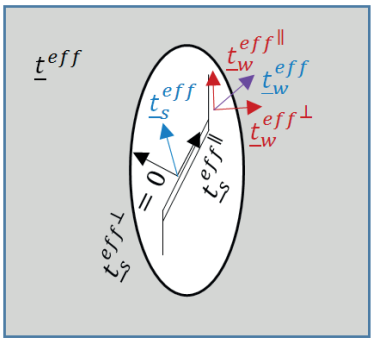

Fig. 6 Components of traction $\underline{t}^{eff}$ in the second sub-problem [19]

$$\underline{t}_w^{eff} \begin{cases} \left(\underline{t}_w^{eff}\right)^{\parallel} = -\left(\underline{t}_w^r\right)^{\parallel} \\ \left(\underline{t}_w^{eff}\right)^{\perp} = -\left(\underline{t}_w^r\right)^{\perp} \end{cases}, \tag{12}$$

Eventually, the effective shear stress mobilized at the micro-crack surface can be calculated by the substitution of Eqs. (8) and (10) into Eq. (11) as follows:

$$\tau_s^{eff} = \tau_c - \mu\left(\sigma_{11}^e cos^2\varphi + \sigma_{22}^e sin^2\varphi + \sigma_{12}^e sin 2\varphi\right) + \frac{1}{2}\left(\sigma_{11}^e - \sigma_{22}^e\right) sin 2\varphi - \sigma_{12}^e cos 2\varphi. \tag{13}$$

2.4 Frictional sliding criterion and flow rule

Under dominated compressive loading with closed micro-cracks, the onset of macroscopically inelastic deformation is typically attributed to the activation of frictional sliding along the micro-cracks, which causes wing cracks to sprout from their tips [19]. According to Zhu et al. (2008, 2011) and Qi et al. (2016), the inelastic deformation caused by frictional sliding along micro-cracks can be treated as plastic strain accompanied with dilatancy in the classic plasticity theory framework, and its evolution can be determined by the normality rule within the thermodynamic framework. For frictional closed cracks, an appropriate criterion, for instance the Coulomb-type criterion, for the onset of frictional sliding along micro-cracks is required. As shown in Fig. 7, an appropriate frictional sliding criterion needs to be formulated at the microscopic scale, which plays the role of the yielding function for plastic strain evolution in the classic theory of plasticity [28]. In this paper, a frictional sliding criterion for micro-cracks is proposed and inelastic deformations originated from frictional sliding along the micro-crack faces are calculated by flow rule and consistency condition in the classic plasticity theory framework. The following general sliding criterion is here assumed that consider both of resisting force (R) and driving force (f) for sliding along micro-crack surfaces:

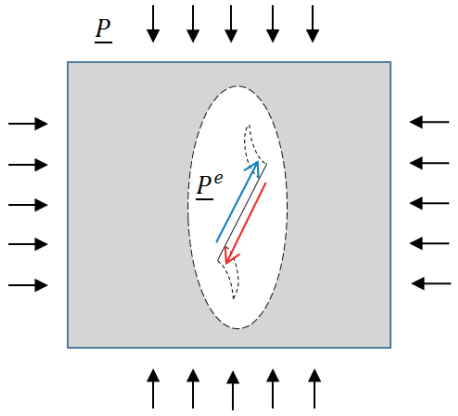

Fig. 7 Plastic strains caused by sliding along micro-cracks [19]

$$g = f(loading) - R(cohesive, friction) \tag{14}$$

where the yield function (g) determines the evolution of frictional sliding along micro-cracks under local stress field ($\underline{P}^e$).

Ayyagari et.al (2018), Liu and Graham-Brady (2016) used the Nemat-Nasser and Obata (1988) approach's to estimate the coefficients of total inelastic strains by equating the force-driven stress intensity factor (K_I), and the displacement-driven stress intensity factor (K_I') [22, 41].

Based on the analysis performed in the previous section, the driving force for frictional sliding along micro-cracks is $(\underline{t}_s^r)^{\|}$. On the other hand, cohesive and frictional resisting forces against sliding along the micro-cracks surfaces can be involved in the resistance function (R) as follows:

$$R = \tau_c - \mu\left(\underline{t}_s^r\right)^{\perp}, \tag{15}$$

where τ_c and μ are cohesion and dry friction coefficient of closed micro-crack respectively. The substitution of driving and resisting forces into Eq. (14) results in the following sliding criterion:

$$g = \left(\underline{t}_s^r\right)^{\|} - \left[\tau_c - \mu\left(\underline{t}_s^r\right)^{\perp}\right] = -\tau_s^{eff}, \tag{16}$$

Also, the substitution of $(\underline{t}_s^r)^{\|}$ and $(\underline{t}_s^r)^{\perp}$ from Eq. (8) leads to the yield function as follows:

$$g = \left(\sigma_{12}^e cos2\varphi + \frac{1}{2}\left(\sigma_{11}^e - \sigma_{22}^e\right) sin2\varphi\right) - \tau_c + \mu\left(\sigma_{11}^e cos^2\varphi + \sigma_{22}^e sin^2\varphi + \sigma_{12}^e sin2\varphi\right), \tag{17}$$

It's noteworthy that the frictional sliding criterion proposed in Eq. (17) is based on the physical facts at the micromechanical scale, for the frictional criterion is formulated using the local stress field. Due to the inelastic deformation arisen from sliding along micro-crack surfaces, the total strain tensor can be decomposed into elastic (ε_{ij}^e) and plastic ($\varepsilon_{ij}^{p^{(sliding)}}$) components:

$$\varepsilon_{ij} = \varepsilon_{ij}^e + \varepsilon_{ij}^{p^{(sliding)}}, \tag{18}$$

$\varepsilon_{ij}^{p^{(sliding)}}$ is induced by frictional sliding along micro-crack surfaces and not based on dislocation in crystalline matrix network. The plastic strain tensor increment ($\dot{\varepsilon}_{kl}^{pl}$) can be obtained from the normality condition of the associated flow rule:

$$\dot{\varepsilon}_{kl}^{pl} = \left(\dot{\lambda}^{pl}\right)^{sliding}\left(\frac{\partial g}{\partial \sigma_{ij}^e}\right), \tag{19}$$

$\left(\dot{\lambda}^{pl}\right)^{sliding}$, is a non-negative multiplier which can be determined by the consistency condition ($g = 0$, $\dot{g} = 0$). Since the frictional sliding criterion $g(\sigma_{11}^e, \sigma_{22}^e, \sigma_{12}^e)$ in Eq. (17) is based on the local stress field applied to the elliptical inclusion, differentiating frictional sliding criterion (g) with respect to the local stress leads to:

$$\begin{bmatrix}\Delta\varepsilon_{11}^{pl}\\ \Delta\varepsilon_{22}^{pl}\\ \Delta\varepsilon_{12}^{pl}\end{bmatrix} = \left(\dot{\lambda}^{pl}\right)^{sliding}\begin{bmatrix}\frac{\partial g}{\partial \sigma_{11}^e}\\ \frac{\partial g}{\partial \sigma_{22}^e}\\ \frac{\partial g}{\partial \sigma_{12}^e}\end{bmatrix} = \left(\dot{\lambda}^{pl}\right)^{sliding}\begin{bmatrix}\mu cos^2\varphi - \frac{1}{2}sin2\varphi\\ \mu sin^2\varphi + \frac{1}{2}sin2\varphi\\ \mu sin2\varphi + cos2\varphi\end{bmatrix} \tag{20}$$

By applying the consistency condition ($dg = \dot{g} = 0$) to the sliding criterion, the plastic multiplier for elastoplastic behaviour condition without damage evolution can be determined as follows:

$$\left(\dot{\lambda}^{pl}\right)^{sliding} = \frac{\frac{\partial g}{\partial \sigma_{ij}^e} E_{ijkl}\dot{\varepsilon}_{kl}}{\frac{\partial g}{\partial \sigma_{ij}^e} E_{ijkl}\frac{\partial g}{\partial \sigma_{kl}^e}}, \tag{21}$$

It's noteworthy that the plastic multiplier is nonnegative under loading and unloading condition. The substitution of the plastic multiplier from Eq. (21) into the incremental stress-strain relation without damage evolution ($\dot{\sigma}_{ij} = E_{ijkl}\dot{\varepsilon}_{kl}^e$) leads to the following fourth order elastoplastic tangential stiffness tensor $E_{ijkl}^{t^{ep}}$ as following:

$$E_{ijkl}^{t^{ep}} = E_{ijkl} - \frac{\left(E_{ijqs}\frac{\partial g}{\partial \sigma_{qs}^e}\right)\otimes\left(E_{klcd}\frac{\partial g}{\partial \sigma_{cd}^e}\right)}{\left(\frac{\partial g}{\partial \sigma_{ij}^e}E_{ijkl}\frac{\partial g}{\partial \sigma_{kl}^e}\right)}, \tag{22}$$

2.5 Damage criterion and damage evolution rule

While the rock material is subjected to compressive loading, sliding along closed initial micro-crack surfaces leads to increase in the stress intensity factor at flaw tips. Subsequently, if the stress intensity factor at flaw tips reaches the fracture toughness, the wing-crack nucleation from flaw tips occurs [23].

Damage in rock materials occurs with wing-crack nucleation, growth and propagation. The damage criterion (F^d) indicating the boundary of damage progression in rock material consists of two principal components of driving and resisting functions. Therefore, it can be expressed in the following general form [30]:

$$F^d = f(loading) - r(resist), \tag{23}$$

where r represents the current resistance to further damage propagation.The driving and resisting functions are the stress intensity factor (K_I) and the mode-I fracture toughness (K_{IC}), respectively. From fracture mechanics viewpoint, damage occurs when the stress intensity factorat flaw tips exceeds the fracture toughness. The mode-I stress intensity factor at the flaw tips for slit-like micro-cracks is suggested by Nemat-Nasser and Horii (1982) [7]:

$$K_I = (K_I)_1 + (K_I)_2 = \frac{-2s\left(t_s^{eff}\right)^{\parallel} \cos\varphi}{\sqrt{\pi\left(l + l^*\right)}} - \left(t_w^{eff}\right)^{\perp} \sqrt{\pi l}, \tag{24}$$

The parameter ($l^* = 0.27s$) is assumed to avoid singularity of $(K_I)_1$ when the wing-cracks are too small ($l = 0$).

Accordingly, $(K_I)_1$ at the flaw tip arises from the resultant shear stress on the closed micro-crack surfaces and subsequently sliding and wedging occur. $(K_I)_2$ arises from the local stress field effect on the wing-crack surfaces embedded in an elliptical inclusion. Wedging effect due to sliding along pre-existing closed micro-crack surfaces is illustrated in Fig. 8(a). Furthermore, Fig. 8(b) depicts a single crack BB' of length $2l$, subjected at its center to a pair of collinear splitting force of same magnitude $F\left(F = -2s\left(t_s^e ff\right)^{\parallel}\right)$. These coupling forces illustrate the representative tension wing-crack BB' influenced by the sliding of pre-existing closed micro-crack AA'.

Substitution of Eqs. (11) and (12) into Eq. (24) leads to express the stress intensity factor (SIF) based on the local stress components:

$$K_I = \frac{-2s\tau^{eff}\cos\varphi}{\sqrt{\pi\left(l + l^*\right)}} - \sigma_{22}^e \sqrt{\pi l}, \tag{25}$$

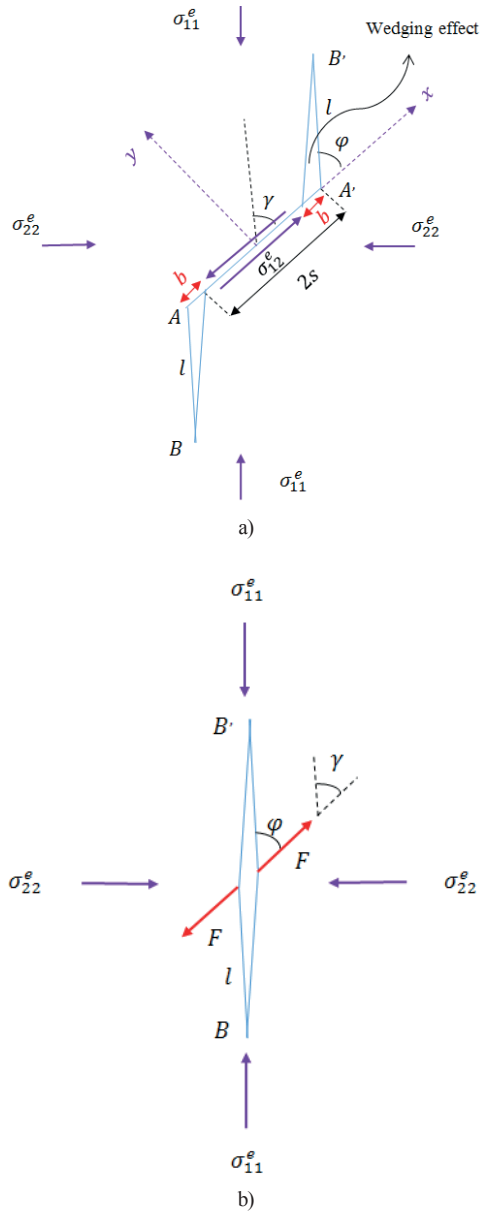

Fig. 8 a) Wedging effect due to sliding along micro-crack surfaces, b) Tension wing-crack subjected to collinear splitting force [31]

As aforementioned, under dynamical loading condition, all of the flaws within the material are approximately activated. The key factor to study the micro-cracks propagation under dynamic loading is dynamic stress intensity factor (K_{ID}) in modeling process. Freund (1972) considered a semi-infinite mode-I crack running in an infinite block of pre-stressed material. In this problem the dynamic stress intensity factor only depends on the current crack tip speed and static stress intensity factor. According to Freund (1972, 1990), the mode-I dynamic stress intensity factor can be determined for propagating flaws as follows [32, 33]:

$$K_{ID} = k\left(\dot{l}\right) K_I, \tag{26}$$

The function $k(\dot{l})$ is a universal function of the propagation rate of micro-cracks tips, which represents the inertial effect on the crack growth [25]:

$$k(\dot{l}) = \left(1 - \frac{\dot{l}}{c_R}\right)\left(1 - \frac{\dot{l}}{2c_R}\right)^{-1} = \frac{2(c_R - \dot{l})}{2c_R - \dot{l}}, \quad (27)$$

here C_R and $\dot{l}$ are the Rayleigh wave speed and the wing-crack tips propagation velocity, respectively. Hence the damage criterion under dynamic loading condition can be expressed as follows:

$$F^d = K_{ID} - K_{IC}, \quad (28)$$

When the damage criterion is satisfied ($F^d = 0$) due to equivalence between fracture toughness (K_{IC}) and dynamic stress intensity factor (K_{ID}), the incremental rate of micro-crack length $\dot{l}$ is determined by substituting Eqs. (26) and (27) in the damage criterion ($F^d = 0$):

$$\dot{l} = c_{max}\left(\frac{K_I - K_{IC}}{K_I - \frac{K_{IC}}{2}}\right)^{\gamma}, \; c_{max} = \frac{c_R}{\alpha}, \quad (29)$$

where c_{max} is the maximum (terminal) speed of a dynamically propagating wing-crack, α and γ are fitting parameters characterizing the toughness-velocity relation. The developed model by Andrew and Ramesh (2016) showed that under dynamic compression, the simulated peak strength is sensitive to the maximum crack growth velocity [29].

2.6 Coupling between frictional sliding and damage evolution

In fact, for most geo-materials, there exists a strong coupling between plastic flow caused by sliding along micro-crack faces and damage evolution due to nucleation and growth of wing-cracks. When frictional sliding and damage evolution take place simultaneously, these two dissipative mechanisms will interfere each other in a strong manner in the sense of the determination of their evolutions. In this paper, the micromechanical damage model of Paliwal and Ramesh (2008) was logically extended by coupling the two dissipative mechanisms, i.e. damage evolution and frictional sliding, for the case of closed micro-cracks. According to the generalized Hook's law, the tensorial stress-strain relation can be written as:

$$\sigma_{ij} = E_{ijkl}\varepsilon^e_{kl}, \quad (30)$$

where E_{ijkl} are the components of the secant stiffness tensor, which vary during the loading process (Carol et al., 2001). Due to simultaneous occurrence of plastic strain increment ($\dot{\varepsilon}^p_{kl}$) and damage evolution ($\dot{E}_{ijkl}$), the incremental stress-strain relation can be obtained by differentiation of Eq. (30) as below:

$$\dot{\sigma}_{ij} = E_{ijkl}\dot{\varepsilon}^e_{kl} + \dot{E}_{ijkl}\dot{\varepsilon}^e_{kl} = E_{ijkl}\dot{\varepsilon}^e_{kl} + \frac{\partial E_{ijkl}}{\partial \Omega}\dot{\Omega}\varepsilon^e_{kl}, \quad (31)$$

The incremental one-dimensional stress- strain diagram with considering plastic strain increment due to frictional sliding along micro-crack surfaces and damage evolution caused by wing-crack propagation is schematically illustrated in Fig. 9.

In Fig. 9, the total strain and stress increments are ($\dot{\varepsilon}$) and ($\dot{\sigma}$) respectively. The total strain increment ($\dot{\varepsilon}$) can be decomposed into elastic and plastic parts. To compute the stress tensor increment in Eq. (31), the damage evolution and plastic flow rule have already been determined by Eqs. (4), (19) and (29). Application of the consistency condition to the frictional sliding criterion in Eq. (17) and using flow rule and the stress-strain relation in Eq. (31) lead to calculate the following plastic multiplier due to frictional sliding along micro-crack surfaces associated with damage evolution:

$$\left(\lambda^{pl}\right)^{damage} = \frac{\frac{\partial g}{\partial \sigma^e_{ij}}\frac{\partial E_{ijkl}}{\partial \Omega}\dot{\Omega}\varepsilon_{kl} - \frac{\partial g}{\partial \sigma^e_{ij}}\frac{\partial E_{ijkl}}{\partial \Omega}\dot{\Omega}\varepsilon^p_{kl} + \frac{\partial g}{\partial \sigma^e_{ij}}E_{ijkl}\dot{\varepsilon}_{kl}}{\frac{\partial g}{\partial \sigma^e_{ij}}E_{ijkl}\frac{\partial g}{\partial \sigma^e_{ij}}}, \quad (32)$$

Because of interaction between damage evolution and plastic flow caused by sliding along micro-cracks, the plastic multiplier calculation in Eq. (32) depends directly

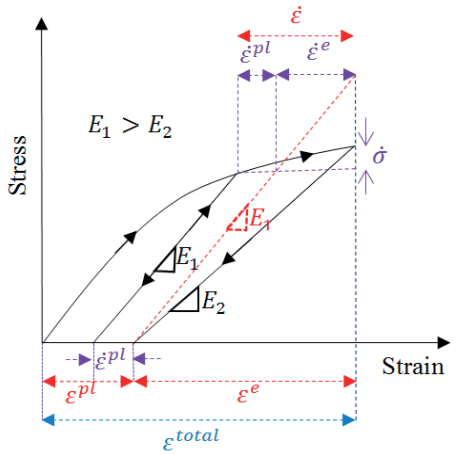

Fig. 9 Schematic illustration of the incremental one-dimensional stress-strain diagram with considering plasticity and damage evolution

on the damage evolution ($\dot{\Omega}$). On the contrary, plasticity has a significant role in damage evolution, for the plastic strain increment due to sliding on micro-crack faces leads to increment of initial micro-crack length by ($\dot{s}$). According to Fig. 8, sliding on initial closed micro-crack faces results in wedging effect and increasing of stress intensity factor at flaw tips.

The increment of initial micro-crack length ($\dot{s}$) due to sliding along micro-cracks is in consistent with a large number of experimental results that secondary cracks always initiate from the tips of the flaws and propagate in a stable manner in a direction coplanar to the flaw. Secondary cracks are always described by many researchers as shear cracks or shear zones as schematically illustrated in Fig. 10 [34, 35].

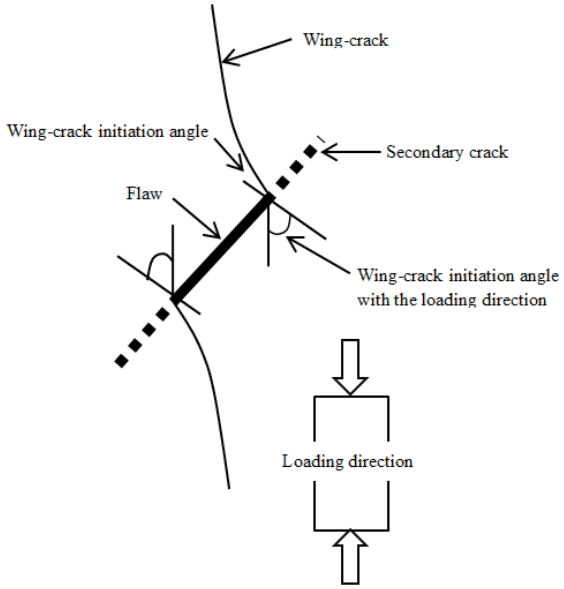

Fig. 10 Simplified crack pattern observed in pre-cracked specimens of rock materials in uniaxial compression [34]

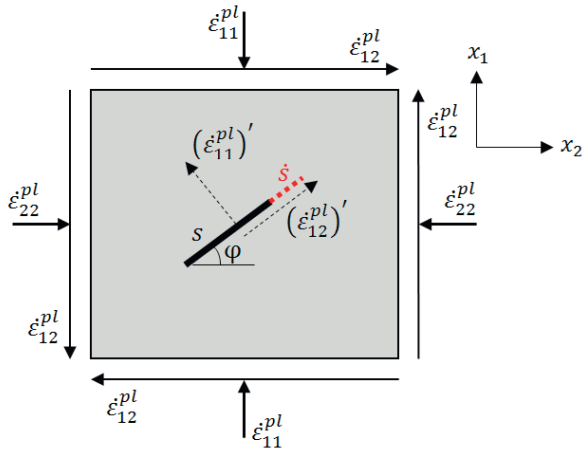

Fig. 11 Increment of initial micro-crack length by ($\dot{s}$)

Secondary cracks play a major role in the cracking process of rocks in compression [36]. Therefore according to Fig. 11, if plastic strain occurs, the increment of initial micro-crack length must be calculated and subsequently stress intensity factor (SIF) is computed by the updated micro-crack length ($s + \dot{s}$).

According to Fig. 11, the plastic strain increments on initial micro-crack surface can be calculated by using strain transformation relations under rotation of axes from global to local corresponding to micro-crack surface. In this regard, the local plastic strains on micro-crack surface can be calculated by the following relations:

$$\begin{aligned}\left(\dot{\varepsilon}_{12}^{pl}\right)' &= -\frac{1}{2}\dot{\varepsilon}_{22}^{pl}sin2\varphi + \frac{1}{2}\dot{\varepsilon}_{11}^{pl}sin2\varphi + \dot{\varepsilon}_{12}^{pl}cos2\varphi \\ \left(\dot{\varepsilon}_{11}^{pl}\right)' &= \dot{\varepsilon}_{22}^{pl}sin^2\varphi + \dot{\varepsilon}_{11}^{pl}cos^2\varphi - \dot{\varepsilon}_{12}^{pl}sin2\varphi,\end{aligned} \tag{33}$$

The shear plastic strain on micro-crack surface leads to increment of initial micro-crack length by ($\dot{s}$). Substitution of the magnitudes ($\dot{\varepsilon}_{11}^{pl}$, $\dot{\varepsilon}_{22}^{pl}$, $\dot{\varepsilon}_{12}^{pl}$) determined from Eq. (20) into Eq. (33) and rearranging yields:

$$\left(\dot{\varepsilon}_{12}^{p}\right)' = \dot{\lambda}^{pl}\left(\frac{3}{2}\mu\ sin2\varphi\ cos2\varphi - \frac{3}{2}\mu\ sin^2 2\varphi + 1\right), \tag{34}$$

The increment of initial micro-crack length ($\dot{s}$) can be calculatedbased on theshear plastic strain increment as follows:

$$\dot{s} = s\left(\dot{\varepsilon}_{12}^{p}\right)' = s\dot{\lambda}^{pl}\left(\frac{3}{2}\mu sin2\varphi cos2\varphi - \frac{3}{2}\mu sin^2 2\varphi + 1\right), \tag{35}$$

where s is the half of the initial micro-crack length.

3 Integrated algorithm and computational procedure

Numerical implementation of the developed micromechanical damage model requires integrating the rate form of the constitutive relations in the finite time step. The classic step by step iterative approach including elastic prediction, plastic and damage corrections was implemented to the numerical computation procedure according to the developed micromechanical damage model. With assuming the increment of total strain at each step, the increments of stress, plastic strain and damage parameter are calculated in each element and added to their previous values based on the constitutive equation in rate form. The step of the numerical computational procedure can be described as follows:

1. The tensors ($\sigma_{ij}^{(n-1)}, \varepsilon_{ij}^{(n-1)}, \varepsilon_{ij}^{e(n-1)}, \varepsilon_{ij}^{p(n-1)}$) and the damage parameter ($\Omega^{(n-1)}$) have been determined at the end of previous step ($n - 1$).

2. Assuming an increment of total strain ($\Delta\varepsilon_{ij}^{(n)}$), the total strain tensor can be calculated as:

$$\varepsilon_{ij}^{(n)} = \varepsilon_{ij}^{(n-1)} + \Delta\varepsilon_{ij}^{(n)} \tag{36}$$

3. The elastic behaviour without plasticity (sliding) and damage process is assumed as the trial elastic prediction:

$$\tilde{\sigma}_{ij}^{(n)} = \sigma_{ij}^{(n-1)} + E_{ijkl}^{(n-1)}\Delta\varepsilon_{kl}^{(n)}, \tag{37}$$

4. The frictional sliding criterion (g) in Eq. (17) and damage criterion ($F^d < 0$) in Eq. (28) are calculated and checked.
5. If ($g < 0$ and $F^d < 0$), the loading applied to rock material is not so high that results in irreversible strain and consequent damage evolution. Therefore, the rock behaviour is elastic, so the calculated trial stress is the real stress.
6. If ($g \geq 0$ and $F^d < 0$), only plastic flow due to sliding on micro-crack surfaces occurs in absence of damage evolution. The plastic multiplier is computed according to Eq. (21). The increment of plastic strain tensor is also calculated based on Eq. (20) and the plastic strain tensor is updated.

In this situation, the plastic strain is only due to sliding on micro-cracks surfaces without damage evolution ($\dot{\Omega} = 0$), so the stress tensor is corrected and updated by using Eqs. (31) and (37) as follows:

$$\sigma_{ij}^{(n)} = \tilde{\sigma}_{ij}^{(n)} - E_{ijkl}^{(n-1)}\Delta\varepsilon_{kl}^{p^{(n)}}, \tag{38}$$

The initial micro-crack length extension due to plastic strain caused by sliding on micro-crack faces is calculated by Eq. (35) and the micro-crack length is updated.

7. If ($g \geq 0$ and $F^d \geq 0$), the plastic flow and damage evolution occur simultaneously. The plastic multiplier, increment of wing-crack length and damage evolution are computed based on Eqs. (32), (29) and (4) respectively. The increment of plastic strain tensor is calculated from Eq. (20) and the damage parameter is updated at n^{th} step. Eventually the stress tensor is corrected based on Eqs. (31) and (37) as follows:

$$\sigma_{ij}^{(n)} = \tilde{\sigma}_{ij}^{(n)} - \frac{\partial E_{ijkl}}{\partial\Omega}\dot{\Omega}^{(n)}\left(\varepsilon_{kl}^{(n-1)} - \varepsilon_{kl}^{pl(n-1)}\right) - E_{ijkl}^{(n-1)}\dot{\varepsilon}_{kl}^{pl(n)}, \tag{39}$$

Increment in micro-crack length due to plastic strain caused by sliding on micro-crack surfaces is computed and then the stress intensity factor (*SIF*) is calculated by the updated micro-crack length.

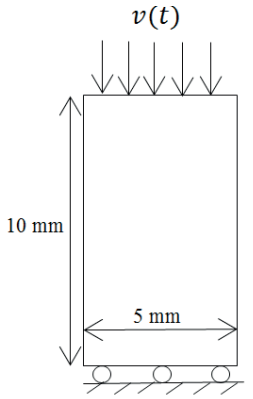

Fig. 12 Schematic illustration of the numerical model under applied velocity field [27]

Table 1 The input flaws characteristic parameters and mechanical properties used in the numerical simulation.

Parameter	Value	Parameter	Value
E(GPa)	36	τ_c	0
v	0.2	(α, γ)	(1,1)
ρ(Kg/m^3)	2600	η(m^{-2})	106
K_{IC}(MPa$\sqrt{\text{m}}$)	0.95	Micro crack length (ηm)	$2s_0 = 50$
μ	0.2	φ	50.7°

4 Numerical simulation results

The main aim of the developed micromechanical model is to reproduce and predict of brittle rock behaviour under dynamic uniaxial compressive loading. The plasticity, damage evolution and the sensitivity of the compressive strength to the applied strain rate are some key features of rock brittle behaviour that are of great interest under dynamic uniaxial compressive loading.

Therefore series of numerical simulations are performed to show the predictive capability of the developed micro-mechanical model. The geometry and boundary condition of the numerical model is shown schematically in Fig. 12. The specified velocity field $v(t)$ is enforced at the upper boundary while a roller boundary condition is placed at the bottom boundary.

The developed micro-mechanical model regarding coupled frictional sliding and damage evolution was programmed into the commercial finite difference environment and implemented in the numerical simulation model by using iterative step by step solution in time scale. Although, the flaws interaction is not considered by direct coalescence of micro-cracks in the numerical simulation, the self-consistent homogenization scheme is used for investigation of damage effect on stress-strain relation. The input flaws characteristic parameters and mechanical properties for a typical rock material used in the numerical

simulation are listed in table 1. It's noteworthy that the fitting parameters (α, γ) are selected as one which are adapted from Paliwal and Ramesh (2008).

The developed micromechanical model regarding coupled frictional sliding along micro-cracks faces and damage evolution was implemented in the numerical simulation to show its advantages in respect to the original micromechanical damage model of Paliwal and Ramesh (2008).

4.1 Imposed strain rate dependency of strength

The numerical simulation is performed by the coupled frictional sliding-micromechanical damage model proposed in this paper to investigate the effects of applied strain rate on peak strength and rock behaviour.

The stress–strain curves are simulated over a range of the imposed strain rates from $\dot{\varepsilon} = 2 \times 10^4$ to $\dot{\varepsilon} = 12 \times 10^4$ 1/s to investigate the variation of the compressive peak strength by the imposed strain rates. The simulated stress-strain curves under various applied strain rates are shown in Fig. 13.

Although Fig. 13 at low strain values shows elastic behaviour with a linear stress–strain relationship, at higher strains the flaws begin to activate by stable crack growth which leads to increase in damage of material. This phenomenon results in stiffness degradation that decreases the slope of the stress–strain curve. When the stress state reaches the peak strength, the slope of the stress–strain curve becomes negative in post-peak region. This post-peak behaviour is most readily related to unstable crack growth and ultimately material macroscopic failure. For the applied strain rates and a given flaws density, the results in Fig. 13 show that the model is capable of predicting damage induced by wing-cracks and plasticity caused by frictional sliding along micro-cracks. Furthermore, an increase in imposed strain rate with the same input flaws parameters leads to increase in the simulated peak strength.

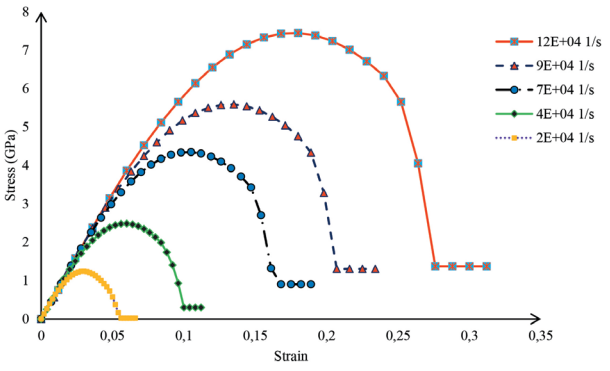

Fig. 13 The stress-strain curves simulated with the developed micromechanical damage model under various applied strain rates

The developed micromechanical model can adequately reproduce many features of the rock behaviour such as the linear elastic, hardening prior to the peak strength and eventually softening at post-peak region. The simulated compressive strength is dramatically sensitive to the imposed strain rate especially in dynamic strain rate ranges. Furthermore, the softening behaviour of material in post-peak region is affected and the material undergoes higher values of strains and damage up to the residual strength (failure).

The fact that flaws have not enough time to grow and propagate under applied high strain rates explains why the peak strength of material increases under dynamic loading by increment of the imposed strain rate.

4.2 Scaling law

Rinehart (1965) found that the dynamic strength of rock exceeded its static strength. His finding has been proved by later experimental observation [37]. This is consistent with the experimentally observed strain rate sensitivity of the compressive strength of various ceramics, e.g. [39] and brittle rocks, e.g. [25]. A scaling relationship is developed by Kimberley et al. (2013) based on the micromechanics of the growth of micro-cracks from populations of pre-existing flaws. The suggested model describes the dynamic compressive strength of brittle materials and captured transitional strain rates in terms of material and microstructural properties [38].

The simulated compressive peak strengths are plotted against the prescribed strain rates in logarithmic scale to investigate the strain rate-sensitivity of the compressive peak strength predicted based on the coupled frictional sliding-micromechanical damage model proposed in this paper as shown in Fig. 14.

According to Fig. 14, variation of the applied strain rate significantly affects the mechanical response of brittle materials. The simulated compressive peak strengths remain nearly constant for the imposed strain rates lower than the transitional strain rate representing the boundary between quasi-static and dynamic loading condition. While the imposed strain rate exceeds the transitional strain rate, the compressive peak strength increases significantly.

In summary, the compressive peak strength slightly increases with increment of the imposed strain rates under quasi-static loading condition, but it considerably rises with increase in the applied strain rate under dynamic loading condition. The aforementioned results indicate that much higher stress is needed under dynamic loading condition to make rock fracture in comparison with static loading condition.

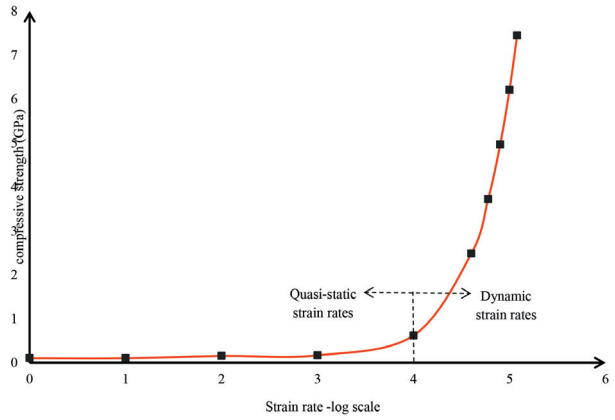

Fig. 14 Variation of the simulated compressive strength with applied strain rate

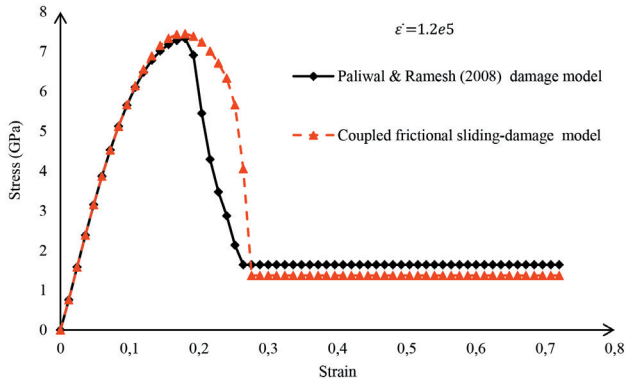

Fig. 15 The comparison of the stress-strain curves simulated by the coupled frictional sliding-damage model and Paliwal and Ramesh (2008) damage model

4.3 Comparison of the developed model and the Paliwal and Ramesh (2008) model

As mentioned before, in the developed micromechanical model the plastic strain caused by frictional sliding along micro-crack surfaces and damage evolution due to wing-crack nucleation are considered simultaneously.

In order to study the effects of plasticity due to frictional sliding along micro-crack faces on rock behaviour, the rock sample was numerically simulated based on the two different constitutive models including the coupled frictional sliding-micromechanical damage model proposed in this paper and the original damage model of Paliwal and Ramesh (2008) under the same imposed strain rate. Fig. 15 shows the two different stress-strain curves simulated by the developed frictional sliding-damage model and the original damage model proposed by Paliwal and Ramesh (2008) under the same imposed strain rate of $\dot{\varepsilon} = 12 \times 10^4$ 1/s.

According to Fig. 15, the simulated stress-strain curves based on the two different constitutive models are approximately similar in pre-peak region, but they are different in post-peak region. In post-peak region the stress-strain curve simulated by the micromechanical damage model of Paliwal and Ramesh (2008) decreases more instantly without considerable increase in strain, indicating more brittle rock behaviour.

On the other hand, the stress-strain curve simulated with the coupled frictional sliding-micromechanical damage model undergoes larger displacements in post-peak region. The area below the post-peak part of the stress-strain diagram represents the energy dissipated by the rock specimen.

As shown in Fig. 15, the energy dissipation by the rock specimen simulated by the micromechanical coupled frictional sliding and damage model is greater than that which is dissipated by the rock specimen simulated with the micromechanical damage model proposed originally by Paliwal and Ramesh (2008).

Therefore, the rock sample simulation with the coupled frictional sliding-micromechanical damage model could increase plasticity and ductility of the rock in post-peak region because of regarding plastic strains caused by the frictional sliding along micro-cracks.

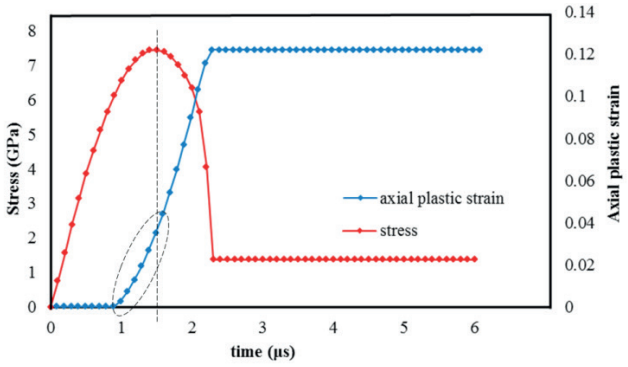

a)

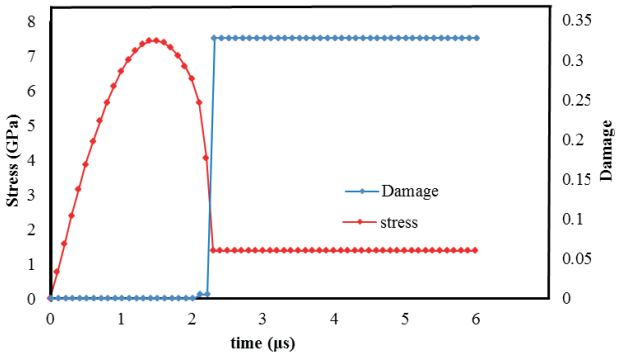

b)

Fig. 16 The simulated stress-strain curves with (a) The plastic strain increment and, (b) Damage evolution

Fig. 16 shows axial plastic strain increment and damage evolution in rock specimen simulated by the coupled frictional sliding-micromechanical damage model proposed in this paper under dynamic uniaxial compressive loading condition.

According to Fig. 16 in the first phase *OA*, the material behaviour remains linear elastic, the stress and strain are linearly related to each other and no plastic strain and damage occur before the activation of sliding along the pre-existing flaws. At this stage, the damage occurrence in material is purely from the pre-existing internal flaws and has very small value. Neither sliding along micro-cracks faces nor damage induced by wing-cracks occur in this phase. The slope of the simulated axial stress-strain curve is the same as the Young's modulus. The phase *AB* corresponds to plastic strain increments as a result of frictional sliding along micro-cracks. In this phase, the progressive accumulation of the frictional sliding leads to the stress concentration at pre-existing flaws tips and increase in the stress intensity factor at this flaws. Once the dynamic stress intensity factor reaches the fracture toughness of the material, in the third phase *BC* the pre-existing micro-cracks will nucleate and develop into wing-cracks and the damage evolution law is activated. The softening behaviour after peak strength because of simultaneous micro-cracks sliding and damage evolution can be seen in Fig. 16(b).

5 Conclusions

In this work, a micromechanical model was developed to take into account the coupling between frictional sliding and damage process under dynamic compressive loading condition. A major feature of the developed model is that the plastic strain caused by frictional sliding along micro-crack surfaces and damage evolution due to wing-crack nucleation are considered simultaneously in a micromechanical model. Micro-crack interactions are considered by means of a self-consistent homogenization scheme in which each micro-crack in ellipsoidal inclusion experiences a local stress field different from the remote stress field acting on isolated micro-cracks. In this paper, the sliding criterion based on the physical facts at the micromechanical scale is proposed in the classic plasticity theory framework associated with the micro-mechanics damage model to simulate the inelastic behaviour of rocks. The developed frictional sliding-damage model algorithm was programmed in the commercial finite difference software environment for numerical simulation of rock material to investigate the relationship between the mechanical behaviour and microstructure of brittle materials and their rate-dependent peak strength under dynamic compressive loading. Variation of the applied strain rate significantly affects the mechanical response of brittle materials. The simulated compressive peak strengths remain nearly constant and insensitive to strain rate for the imposed strain rates below the transitional strain rate representing the boundary between quasi-static and dynamic loading condition. While the imposed strain rate exceeds the transitional strain rate, the compressive peak strength increases dramatically. On the other hand, the rock sample simulation with the coupled frictional sliding-damage model could increase plasticity and ductility of the rock in post-peak region because of regarding plastic strains caused by the frictional sliding along micro-cracks. Furthermore, the axial plastic strain increment and damage evolution in rock specimen were recorded during numerical simulation by the proposed coupled frictional sliding-micromechanical damage model under dynamic uniaxial compressive loading condition. The progressive accumulation of the frictional sliding leads to the stress concentration at the pre-existing flaws tips. This phenomenon leads to increase in the stress intensity factor at the flaws tips.

References

[1] Qi, M., Shao, J. F., Giraud, A., Zhu, Q. Z., Colliat, J. B. "Damage and plastic friction in initially anisotropic quasi brittle materials", International Journal of Plastic, 82, pp. 260–282, 2016. https://doi.org/10.1016/j.ijplas.2016.03.008

[2] Wong, T.-F. "Micromechanics of faulting in Westerly granite", International Journal of Rock Mechanics and Mining Science & Geomechanics Abstracts, 19(2), pp. 49–62, 1982. https://doi.org/10.1016/0148-9062(82)91631-X

[3] Fredrich, J. T., Evans, B., Wong, T.-F. "Micromechanics of the brittle to plastic transition in Carraramarble", Journal of Geophysics and Research: Solid Earth, 94(B4), pp. 4129–4145, 1989. https://doi.org/10.1029/JB094iB04p04129

[4] Liu, J., Graham-Brady, L. "Effective anisotropic compliance relationships for wing-cracked brittle materials under compression", International Journal of Solids and Structure, 100–101, pp. 151–168, 2016. https://doi.org/10.1016/j.ijsolstr.2016.08.012

[5] Chen, W., Ravichandran, G. "Static and dynamic compressive behaviour of aluminum nitride under moderate confinement", Journal of the American Ceramic Society, 79(3), pp. 579–584, 1996. https://doi.org/10.1111/j.1151-2916.1996.tb07913.x

[6] Yuan, X. P., Liu, H. Y., Wang, Z. Q. "An interacting crack- mechanics based model for elastoplastic damage model of rock-like materials under compression", International Journal of Rock Mechanics and Mining Sciences,58, pp. 92–102, 2013. https://doi.org/10.1016/j.ijrmms.2012.09.007

[7] Nemat-Nasser, S., Horii, H. "Compression-induced nonplanar crack extension with application to splitting, exfoliation, and rock burst", Journal of Geophysics and Research: Solid Earth, 87(B8), pp. 6805–6821, 1982. https://doi.org/10.1029/JB087iB08p06805

[8] Nemat-Nasser, S., Deng, H. "Strain-rate effect on brittle failure in compression", Acta Metallurgicaet et Materialia, 42(3), pp. 1013–1024, 1994. https://doi.org/10.1016/0956-7151(94)90295-X

[9] Krajcinovic, D. "Damage mechanics", 1st ed., Elsevier, Amsterdam, The Netherlands, 1996.

[10] Kachanov, M. L. "A microcrack model of rock inelasticity part I: Frictional sliding on microcracks", Mechanics of Materials, 1(1), pp. 19–27, 1982. https://doi.org/10.1016/0167-6636(82)90021-7

[11] Renaud, V., Kondo, D., Henry, J. P. "Computation of effective moduli for microcracked materials: a boundary element approach", Computational Materials Science, 5(1–3), pp. 227–237, 1996. https://doi.org/10.1016/0927-0256(95)00074-7

[12] Andrieux, S., Bamberger, Y., Marigo, J.-J. "Model of microcracked material for concrete and rocks", Journal de Mecanique Theorique et Appliquee, 5(3), pp. 471–513, 1986. Available at https://www.researchgate.net/publication/265370454 [Accessed: 16.11.2018]

[13] Gambarotta, L., Lagomarsino, S. "A microcrak damage model for brittle materials", International Journal of Solids and Structure, 30(2), pp. 177–198, 1993. https://doi.org/10.1016/0020-7683(93)90059-G

[14] Pensée, V., Kondo, D. "A 3-D micromechanical analysis of damage by mesocracking", Comptes Rendus de l'Académie des Sciences - Series IIB - Mechanics, 329(4), pp. 271–276, 2001.

[15] Mori, T., Tanaka, K. "Averages stress in matrix and average elastic energy of materials with misfitting inclusions", Acta Metallurgica, 21(5), pp. 571–574, 1973. https://doi.org/10.1016/0001-6160(73)90064-3

[16] Castañeda, P. P., Willis, J. R. "The effect of spatial distribution on the behaviour of composite materials and cracked media", Journal of the Mechanics and Physics of Solids, 43(12), pp. 1919–1951, 1995. https://doi.org/10.1016/0022-5096(95)00058-Q

[17] Zhu Q. Z., Kondo D., Shao J. F. "Micromechanical analysis of coupling between anisotropic damage and friction in quasi brittle materials: Role of homogenization scheme", International Journal of Solids and Structures, 45(5), pp. 1358–1405, 2008. https://doi.org/10.1016/j.ijsolstr.2007.09.026

[18] Zhu Q. Z., Shao J. F., Kondo D. "A micromechanics-based thermodynamic formulation of isotropic damage with unilateral and friction effects", European Journal of Mechanics - A/Solids, 30(3), pp. 316–325, 2011. https://doi.org/10.1016/j.euromechsol.2010.12.005

[19] Paliwal, B., Ramesh, K. T. "An interacting micro-crack damage model for failure of brittle materials under compression", Journal of the Mechanics and Physics of Solids, 56(3), pp. 896–923, 2008. https://doi.org/10.1016/j.jmps.2007.06.012

[20] Graham-Brady, L. "Statistical characterization of meso-scale uniaxial compressive strength in brittle materials with randomly occurring flaws", International Journal of Solids and Structures, 47(18–19), pp. 2398–2413, 2010. https://doi.org/10.1016/j.ijsolstr.2010.04.034

[21] Liu, J. "Micro-mechanical modeling of brittle materials under dynamic compressive loading", Ph.D. Thesis, Johns Hopkins University, 2015.

[22] Ayyagari, R. S., Daphalapurkar, N. P., Ramesh, K. T. "The effective compliance of spatially evolving planar wing-cracks", Journal of the Mechanics and Physics of Solids, 111, pp. 503–529, 2018. https://doi.org/10.1016/j.jmps.2017.11.016

[23] Hu, G., Liu, J., Graham-Brady, L., Ramesh, K. T. "A 3D mechanistic model for brittle materials containing evolving flaw distributions under dynamic multiaxial loading", Journal of the Mechanics and Physics of Solids 78, pp. 269–297, 2015. https://doi.org/10.1016/j.jmps.2015.02.014

[24] Gross, D., Seelig, T. "Fracture mechanics with an introduction to micromechanics", Springer, Berlin, Germany, 2011.

[25] Huang, C., Subhash, G. "Influence of lateral confinement on dynamic damage evolution during uniaxial compressive response of brittle solids", Journal of the Mechanics and Physics of Solids, 51(6), pp. 1089–1105, 2003. https://doi.org/10.1016/S0022-5096(03)00002-4

[26] Daphalapurkar, N. P., Ramesh, K. T., Graham-Brady, L., Molinari, J.-F. "Predicting variability in the dynamic failure strength of brittle materials considering pre-existing flaws", Journal of the Mechanics and Physics of Solids, 59(2), pp. 297–319, 2011. https://doi.org/10.1016/j.jmps.2010.10.006

[27] Katcoff, C. Z., Graham-Brady, L. L. "Modeling dynamic brittle behaviour of materials with circular flaws or pores", International Journal of Solids and Structures, 51(3–4), pp. 754–766, 2014. https://doi.org/10.1016/j.ijsolstr.2013.11.004

[28] Xie, N., Zhu, Q. Z., Xu, L. H., Shao, J. F. "A micromechanics-based elastoplastic damage model for quasi-brittle rocks", Computers and Geotechnics, 38(8), pp. 970–977, 2011. https://doi.org/10.1016/j.compgeo.2011.07.014

[29] Tonge, A. L., Ramesh, K. T. "Multi-scale defect interactions in high-rate failure of brittle materials, Part II: Application to design of protection materials", Journal of the Mechanics and Physics of Solids, 86, pp. 237–258, 2016. https://doi.org/10.1016/j.jmps.2015.10.006

[30] Shao, J. F., Jia, Y., Kondo, D., Chiarelli, A. S. "A coupled elastoplastic damage model for semi-brittle materials and extension to unsaturated conditions", Mechanics of Materials, 38(3), pp. 218–232, 2006. https://doi.org/10.1016/j.mechmat.2005.07.002

[31] Horii, H., Nemat-Nasser, S., Ashby, M. F. "Brittle failure in compression: splitting, faulting and brittle-ductile transition", Philosophical transactions of the royal society, 319(1549), pp. 337–374, 1986. https://doi.org/10.1098/rsta.1986.0101

[32] Freund, L. B. "Crack propagation in an elastic solid Subjected to general loading-II. Non-uniform rate of extension", Journal of the Mechanics and Physics of Solids, 20(3), pp. 129–140, 1972. https://doi.org/10.1016/0022-5096(72)90006-3

[33] Freund, L. B. "Dynamic fracture mechanics", Cambridge University Press, New York City, N.Y., U.S.A. 1990.

[34] Bobet, A., Einstein, H. H. "Fracture coalescence in rock-type materials under uniaxial and biaxial compression", International Journal of Rock Mechanics and Mining Sciences, 35(7), pp. 863–888, 1998. https://doi.org/10.1016/S0148-9062(98)00005-9

[35] Bobet, A. "The initiation of secondary cracks in compression", Engineering Fracture Mechanics, 66(2), pp. 187–219, 2000. https://doi.org/10.1016/S0013-7944(00)00009-6

[36] Wong, R. H. C., Chau, K. T. "Crack coalescence in a rock-like material containing two cracks", International Journal of Rock Mechanics and Mining Sciences, 35(2), pp. 147–164, 1998. https://doi.org/10.1016/S0148-9062(97)00303-3
[37] Zhang, Z.-X. "Rock Fracture and Blasting: Theory and Applications", 1st ed., Butterworth-Heinemann, Oxford, United Kingdom , 2016.
[38] Kimberley, J., Ramesh, K. T., Daphalapurkar, N. P. "A scaling law for the dynamic strength of brittle solids", Acta Materialia, 61(9), pp. 3509–3521, 2013. https://doi.org/10.1016/j.actamat.2013.02.045
[39] Lankford, J. "High strain rate compression and plastic flow of ceramics", Journal of Materials Science Letters, 15(9), pp. 745–750, 1996. https://doi.org/10.1007/BF00274593
[40] Nemat-Nasser, S., Obata, M. "A microcrack model of dilatancy in brittle materials", Journal of Applied Mechanics, 55(1), pp. 24–35, 1988. https://doi.org/10.1115/1.3173647
[41] Liu, J., Graham-Brady, L. "Effective anisotropic compliance relationships for wing-cracked brittle materials under compression", International Journal of Solids and Structures, 100–101, pp. 151–168, 2016. https://doi.org/10.1016/j.ijsolstr.2016.08.012
[42] Ván, P., Vásárhelyi, B. "Sensitivity analysis of GSI based mechanical parameters of the rock mass", Periodica Polytechnica Civil Engineering, 58(4), pp. 379–386, 2014. https://doi.org/10.3311/PPci.7507
[43] Ghasempour, N., Moosavi, M., Aghighi, M. A. "A Micromechanical Model to Estimate Borehole Collapse Pressure", Periodica Polytechnica Civil Engineering, 61(3), pp. 581–589, 2017. https://doi.org/10.3311/PPci.9979
[44] Vásárhelyi, B., Kovács, D. "Empirical methods of calculating the mechanical parameters of the rock mass", Periodica Polytechnica Civil Engineering, 61(1), pp. 39–50, 2017. https://doi.org/10.3311/PPci.10095

Appendix A.
Calculation of local stress field at elliptical inclusion boundary

Consider a slit-like flaw is assumed in elliptical inclusion of an undamaged, pristine isotropic material surrounded by micro-cracked matrix under uniaxial compressive loading. The regions around the elliptical inclusion are damaged and homogenized by the self-consistent homogenization scheme. The resulting mismatch of effective elastic properties of the micro-cracked media and the pristine material at the elliptical inclusion boundary leads to the local stresses filed ($\underline{P}_e$) applied to the elliptical inclusion that differ from the remote compressive loading ($\underline{P}$). According to Fig. 2, the effective homogenized module $\bar{E}$ can be obtained based on the self-consistent homogenization scheme by the following equation:

$$\bar{\mathbb{E}} = \mathbb{E}\left(1-\frac{\pi^2}{30}(1-v)(5-4v)\Omega\right), \tag{A 1}$$

The local stresses filed ($\underline{P}_e$) and the remote compressive loading ($\underline{P}$) are related to each other by:

$$\underline{\underline{B}} = \left\{[\mathbb{I}]+[\mathbb{C}^*][\mathbb{C}^I]^{-1}\right\}^{-1}\left\{[\mathbb{I}]+[\mathbb{C}^*][\mathbb{C}^M]^{-1}\right\}, \tag{A 2}$$

where $[\mathbb{I}]$ is the 3 × 3 identity tensor, and $[\mathbb{C}^I]$ is undamaged constitutive tensor.

$$[\mathbb{C}^I] = \frac{\mathbb{E}}{(1+v)(1-2v)}\cdot\begin{bmatrix}1-v & v & v\\ v & 1-v & v\\ v & v & 1-v\end{bmatrix}, \tag{A 3}$$

$[\mathbb{C}^M]$ is the constitutive tensor for the damaged matrix material:

$$[\mathbb{C}^M] = \frac{\bar{\mathbb{E}}}{(1+v)(1-2v)}\cdot\begin{bmatrix}1-v & v & v\\ v & 1-v & v\\ v & v & 1-v\end{bmatrix}, \tag{A 4}$$

and $[\mathbb{C}^*]$ is defined as:

$$[\mathbb{C}^*] = [\mathbb{C}^M][\mathbb{S}]^{-1}([\mathbb{I}] - [\mathbb{S}]) \tag{A 5}$$

where $[\mathbb{S}]$ is the Eshelby tensor for an ellipsoidal inclusion in a matrix, defined as follows:

$$[\mathbb{S}] = \begin{bmatrix}S_{11} & S_{12} & S_{13}\\ S_{21} & S_{22} & S_{23}\\ S_{31} & S_{32} & S_{33}\end{bmatrix}, \tag{A 6}$$

in which the 1-direction is in the direction of the uniaxial compressive loading as well as the major axis of the ellipsoidal inclusion, and the 2- and 3- directions are perpendicular to the 1-direction and each other. The nine components of $[\mathbb{S}]$ are:

$$\begin{aligned}
S_{12} = S_{13} &= \frac{1-2v}{4(1-v)}\left(\frac{a}{b}\right)^2(I_2 - I_3)\\
&+\frac{v}{2(1-v)}\left(\frac{a}{b}\right)^4(I_1 - 2I_2 + I_3),\\
S_{31} = S_{21} &= \frac{v}{4(1-v)}I_3 + \frac{1}{4}\left(\frac{a}{b}\right)^2(I_2 - I_3),\\
S_{22} = S_{33} &= \frac{5-4v}{16(1-v)}I_3 + \frac{2-v}{4(1-v)}\left(\frac{a}{b}\right)^2(I_2 - I_3),\\
S_{23} = S_{32} &= \frac{4v-1}{16(1-v)}I_3 + \frac{v}{4(1-v)}\left(\frac{a}{b}\right)^2(I_2 - I_3).
\end{aligned} \tag{A 7}$$